

Journal of Composite Materials

<http://jcm.sagepub.com/>

Experimental evaluation and statistical characterization of the strength and strain energy density distribution of Kevlar KM2 yarns: exploring length-scale and weaving effects

Gaurav Nilakantan, Ahmad Abu Obaid, Michael Keefe and John W. Gillespie, Jr.

Journal of Composite Materials published online 8 November 2010

DOI: 10.1177/0021998310387667

The online version of this article can be found at:

<http://jcm.sagepub.com/content/early/2010/11/02/0021998310387667>

Published by:



<http://www.sagepublications.com>

On behalf of:



[American Society for Composites](http://www.americansocietyforcomposites.com)

Additional services and information for *Journal of Composite Materials* can be found at:

Email Alerts: <http://jcm.sagepub.com/cgi/alerts>

Subscriptions: <http://jcm.sagepub.com/subscriptions>

Reprints: <http://www.sagepub.com/journalsReprints.nav>

Permissions: <http://www.sagepub.com/journalsPermissions.nav>

Experimental evaluation and statistical characterization of the strength and strain energy density distribution of Kevlar KM2 yarns: exploring length-scale and weaving effects

Gaurav Nilakantan^{1,2}, Ahmad Abu Obaid¹, Michael Keefe^{1,3}
and John W. Gillespie Jr^{1,2,4}

Journal of Composite Materials

0(0) 1–21

© The Author(s) 2010

Reprints and permissions:

sagepub.co.uk/journalsPermissions.nav

DOI: 10.1177/0021998310387667

jcm.sagepub.com



Abstract

This article experimentally investigates the tensile strength distributions of 600 den Kevlar KM2 yarns under quasi-static tensile loading. The strength distributions were best characterized using the 3-parameter Weibull and generalized Gamma distributions. In order to assess the effects of weaving on the strength distributions, Kevlar yarns were tested from a spool and then compared to yarns extracted from greige and scoured Kevlar fabrics. The weaving process and treatments caused various levels of strength degradation which shifted the strength distributions toward lower strengths. The warp yarns were degraded to a greater extent than the fill yarns. The scouring process induced further strength degradations in the woven fabric. Length-scale effects were studied by using gage lengths varying between 25.4 and 381.0 mm. The strength distributions were observed to shift toward lower strengths with increasing gage lengths. A new distribution function based on a modification to the 3-parameter Weibull distribution is proposed to account for length-scale effects. In addition to the strength distributions, the experimental load–extension plots are used to compute the strain energy density or work-to-break values normalized by the yarn volume, which are then statistically characterized and analyzed in a similar manner.

Keywords

polymer, Kevlar KM2, tensile testing, yarn strength, statistical analysis, cumulative distribution function, length scale, weaving effects

Introduction

Certain materials such as poly(p-phenylene terephthalamide) (Aramid, e.g., Kevlar, Twaron), poly(p-phenylene benzobisoxazole) (PBO, e.g., Zylon), and ultra-high molecular weight polyethylene (UHMWPE, e.g., Spectra, Dyneema) have high strength, high stiffness, and high strength-to-weight ratios, making them ideal in applications requiring impact and penetration resistance against incident high-energy projectiles. These applications include flexible protective clothing for law enforcement and military personnel, turbine fragment containment, and spall liners in infantry vehicles. For such applications, these materials are often used in the form of continuous filaments. These filaments are bundled together to form yarns that are further woven into 2D and 3D fabrics, or to form

unidirectional tows that are laid as plies in composites structures. The impact performance of these textile structures is probabilistic in nature and best characterized using statistical methods. The probabilistic nature

¹Center for Composite Materials, University of Delaware, Newark, DE 19716, USA.

²Department of Materials Science and Engineering, University of Delaware, Newark, DE 19716, USA.

³Department of Mechanical Engineering, University of Delaware, Newark, DE 19716, USA.

⁴Department of Civil and Environmental Engineering, University of Delaware, Newark, DE 19716, USA.

Corresponding author:

John W. Gillespie Jr, Center for Composite Materials, University of Delaware, Newark, DE 19716, USA

Email: gillespi@udel.edu

of impact performance arises from various sources of which the material variability in tensile performance is one factor. The tensile performance is controlled by parameters such as the filament and yarn tensile modulus and strength. For example, it is expected that an impacting projectile engaged by the stronger yarns of a fabric structure would result in an increased impact performance over a projectile engaging weaker yarns. However, there are other parameters to consider such as filament–filament frictional interactions which could improve the tensile performance of yarns, just as yarn–yarn frictional interactions could improve the tensile performance of fabrics.

Experimental testing has shown that the tensile strength of monofilaments comprised of materials such as Kevlar, alumina, silicon carbide, and carbon under quasi-static and high-rate loading conditions is statistical in nature, and can be well characterized using certain statistical distributions such as the 2-parameter Weibull distribution.^{1–9} Consequently, it follows that the tensile strength of filament bundles or yarns also follows a statistical distribution. The source of the variability in filament strength arises due to the presence of flaws or defects along the filament length and the nonconstant cross-sectional area that varies along the length. Interestingly, many of these filaments also display a length-scale effect, wherein the strength is observed to decrease with increasing gage lengths. This is mainly attributed to the greater probability of locating a critical defect along the gage length as it increases. Consequently, the strength distribution of yarns also exhibits length-scale effects. Often modifications to the Weibull distribution are used to characterize the strength distributions as a function of gage length.^{4,7,10,11}

The tensile strength distributions of filaments and yarns are degraded by environmental factors such as exposure to extreme temperatures, humidity, and ultra-violet radiation.^{12–17} Another source of strength degradation is the weaving process used to weave the yarns into a fabric. Mechanisms of weaving damage are due to monofilament breakage and abrasion caused by relative sliding between the yarns and the loom machinery, and between the warp and fill yarns, which in turn are governed by the tension and velocity settings employed during weaving.^{18,19} Large curvature induced compressive kink banding in the undulating warp and fill yarns, especially in the through-thickness or z-tows in 3D fabrics can also degrade the strength.^{9,20,21} Figure 1 shows a scanning electron microscope (SEM) image at a magnification of 2500× that displays possible damage mechanisms, as highlighted by the bold arrows, in the filaments of a 600 den Kevlar KM2 yarn. This includes compressive kink bands along the filament length, which could be caused by large curvatures or compressive strains in the filament. In addition, fibrillation is observed in one filament where the skin structure shows signs of fibril peeling, leaving behind grooves on the surface, which could be caused by abrasion. The net effects of these degradation mechanisms are quantified by the shift in the strength distributions to lower strength levels compared to the control samples.

In this article, we study the statistical tensile strength distribution of 600 den Kevlar KM2 yarns under quasi-static tensile loading conditions. The effects of gage length on the strength distributions are assessed by varying the length between 25.4 and 381.0 mm. Weaving strength degradations are assessed by comparing the strength distributions of yarns from the spool

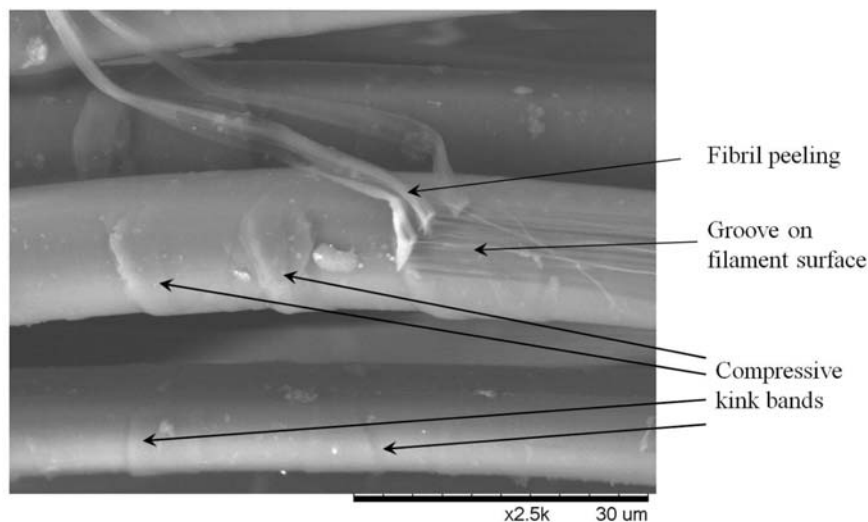


Figure 1. SEM image showing damage mechanisms in the filaments of a 600 den Kevlar KM2 yarn.

which serve as the control sample, against warp and fill yarns extracted from greige and scoured Kevlar S706 (*S=Style*) fabrics. In addition to the tensile strengths, the work-to-break values normalized by the yarn volume, or strain energy densities (SEDs; with units of mJ/mm^3 or N/mm^2) are also statistically characterized using the experimental load–displacement curves. Length-scale and weaving effects based on SED data are then compared against those based on strength data.

Experimental methodology for the quasi-static tensile testing of yarns

Three sources of continuous filament Kevlar KM2 yarns were selected for this study. The Kevlar yarns were manufactured by DuPont. Each yarn comprises of 400 circular filaments of approximately $12\ \mu\text{m}$ diameter with a density of $1.44\ \text{g}/\text{cm}^3$ as reported by the manufacturer. The first source comprised of 600 den Kevlar KM2 yarns obtained from a spool, which serves as the control sample. The other two sources respectively comprised of greige and scoured Kevlar S706 fabrics, from which warp and fill yarns were manually extracted very carefully so as not to cause any damage. The fabrics were woven by the Hexcel Corporation. Kevlar S706 is a plain weave fabric comprised of these 600 den Kevlar KM2 yarns, with a count of 34 yarns/in. in the warp and fill directions, and an areal density of $180\ \text{g}/\text{m}^2$. Figure 2 displays fabric micrograph images of the yarn cross-sectional shapes and yarn undulations as seen from the warp and fill directions. The warp yarns have a greater degree of undulations or larger curvature than the fill yarns. Figure 3 displays a SEM image of the Kevlar filaments within the yarn, at a magnification of $350\times$. Greige fabric refers to the woven fabric fresh off the loom while scoured fabric refers to a greige fabric that has been mechanically washed repeatedly in a hot solution of water and certain proprietary additives

which vary from one commercial weaver to the next. Scouring is done to remove any foreign particles and broken monofilaments from the fabric, to remove any surface treatments added to the yarns prior to weaving, as well as to alter or improve the surface behavior of the fabrics making them amenable to further surface treatments. All materials were received in an ‘as-is’ condition from the Army Research Lab (ARL), Aberdeen Proving Grounds, MD, USA.

The denier of the yarns from the spool and extracted from the fabrics were calculated by weighing at least 30 samples of gage lengths 254.0, 381.0, and 508.0 mm from each yarn source. Table 1 reports the measured denier of these yarns from each source. The denier is defined as the weight in grams of 9000 m of the yarn material. The measured denier of the spool yarns was 2.2% higher than the manufacturer-reported value of 600. The measured denier of the greige warp yarns was the highest of all, about 2.0% higher than the measured spool yarn denier and 4.2% higher than the

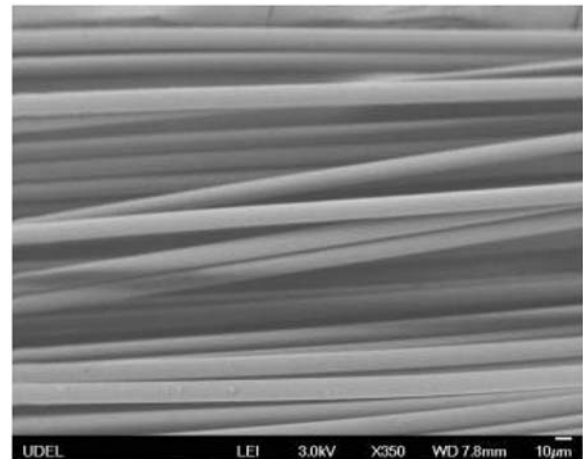


Figure 3. SEM image of filaments within the 600 den Kevlar KM2 yarn.

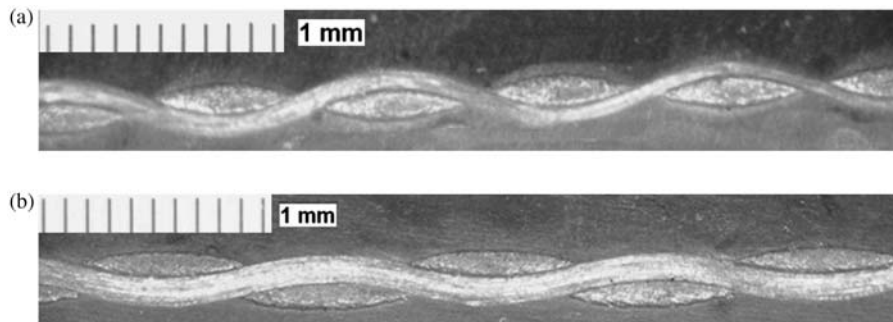


Figure 2. Micrographs of the Kevlar S706 fabric: (a) warp trajectory with fill cross-sections and (b) fill trajectory with warp cross-sections.

manufacturer reported spool yarn denier. This is consistent with the fact that many commercial weavers apply spin-finish and surface treatments, especially to the warp yarns, prior to weaving in an attempt to reduce friction and minimize surface abrasion. As seen in Table 1, the measured deniers of the scoured warp and fill yarns were very close to 600 indicating the scouring process has removed almost all of the previously applied spin-finish and surface treatments. The gage lengths chosen for the spool yarns were 25.4, 50.8, 101.6, 254.0, and 381.0 mm while those for the yarns extracted from the fabrics were 25.4, 50.8, 101.6, and 381.0 mm. All yarn samples were end-tabbed, see Figure 4(a). The end-tabbing method was preferred over using Bollard-type jaws since the yarn gage lengths could be accurately assessed which was important for studying length-scale effects. The minimum gage length possible with the Bollard-type jaws was also limited to around 150 mm; however, samples as small as 25.4 mm could be prepared using end-tabbing. Before testing, all end-tabbed samples were placed

for a minimum of 15 h in a vacuum oven maintained at room temperature. An Instron Model 5567 with a ± 500 N load cell was used for testing, see Figure 4(b). In accordance with ASTM standard D7269-07 ‘Standard Test Methods for Tensile Testing of Aramid Yarns,’ the cross-head speed for the quasi-static tensile testing in in./min was set at 50% of the gage length in inches, which corresponds to a strain rate of 0.5 min^{-1} . Yarns were tested at room temperature with no twist imparted. For each tensile test, the peak tenacity (in g/den) and load–displacement response (N–mm) were recorded. The tenacity data were then converted into tensile strength data with SI units of MPa using the following relation:

$$\text{Strength (MPa)} = 88.26 \times \text{Tenacity (g/den)} \times \text{Density (g/cm}^3\text{)} \quad (1)$$

with the Kevlar KM2 density set at the manufacturer reported value of 1.44 g/cm^3 . Thus, the yarn tensile strength calculated using Equation (1) is based on the actual filament area, and does not consider the increase in yarn denier (Table 1), beyond the manufacturer reported nominal value of 600, due to the additional yarn spin-finish and surface treatments.

The effects of machine compliance were removed from all the displacement data needed for accurate work-to-break or strain energy calculations. In order to calculate the machine compliance, following ASTM Standard 3379-75 ‘Standard Test Method for Tensile Strength and Young’s Modulus for High-Modulus Single-Filament Materials,’ the inverse of the average load (N)–displacement (mm) slopes were

Table 1. Yarn denier measurements

Source	Denier	SD
Spool	613	2.47
Greige warp	625	4.71
Greige fill	610	2.82
Scoured warp	601	5.30
Scoured fill	605	2.00

SD, standard deviation.

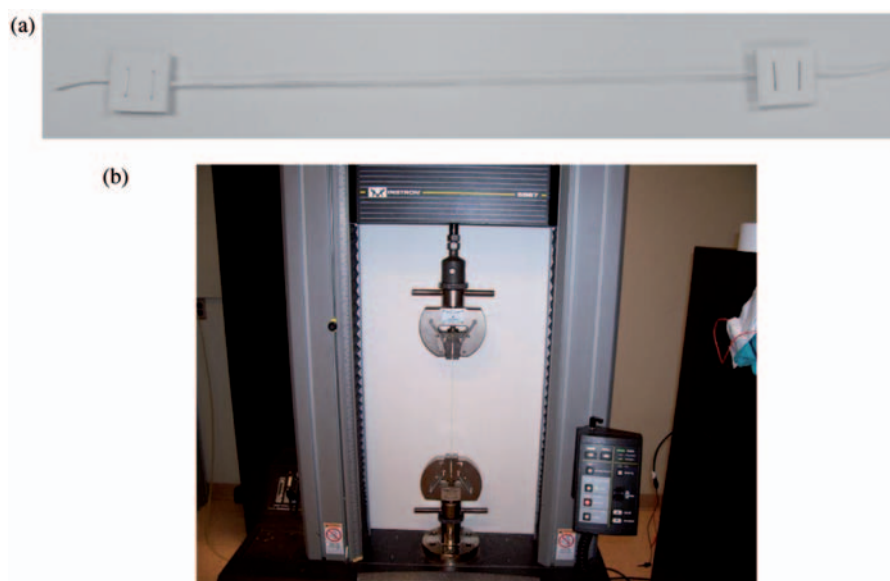


Figure 4. Experimental set-up of: (a) end-tabbed yarn sample and (b) Instron Model 5567 with fixtures and yarn sample.

plotted as a function of gage length for each yarn source as shown in Figure 5. Then the y -intercept of the fitted linear trend line of the form $y = mx + c$ ($m = \text{slope}$ and $c = \text{intercept}$) yields the machine

compliance, as shown in Figure 5. The machine compliance was obtained as follows for each yarn source tested: 0.0050 mm/N (spool), 0.0056 mm/N (greige warp), 0.0052 mm/N (greige fill), 0.0072 mm/N (scoured warp), and 0.0072 mm/N (scoured fill).

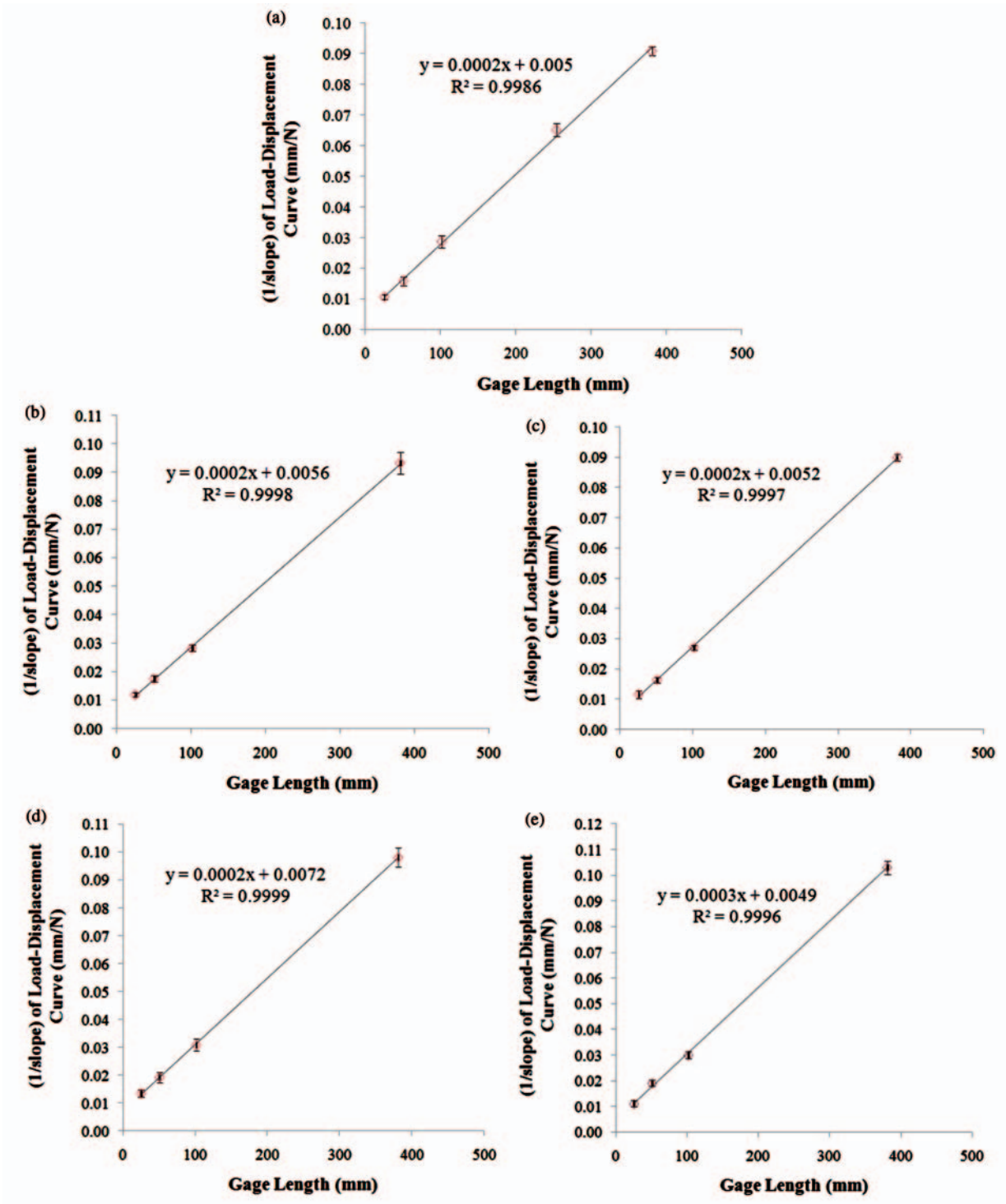


Figure 5. Machine compliance calculations for data sets using: (a) spool, (b) greige warp, (c) greige fill, (d) scoured warp, and (e) scoured fill.

(scoured warp), and 0.0049 mm/N (scoured fill). As expected, the calculated machine compliances were consistent for all yarn sources end-tabbed using similar cardboard tabs except for the scoured warp yarn samples which were end-tabbed with thicker cardboard tabs. Most importantly, the correlation coefficient for all machine compliance data was in the range 0.9986–0.9999 ensuring accurate load–extension measurements. For each set of tests, at least 30 data points were generated in order to perform the statistical analysis.

Statistical analysis techniques

For each set of experimental tests, the strengths are arranged in an increasing order of magnitude and assigned median ranks (MRs), given by:

$$\text{MR} = \frac{i - 0.3}{N + 0.4} \quad (2)$$

where i is the sample number and N the sample size. Each MR yields the cumulative probability of failure at that particular strength. Next, a parametric cumulative distribution function (CDF) needs to be generated in order to fit this MR data. Different forms of the Weibull distribution are often used in these types of studies.^{4,7,8,22,23} In order to select those distributions that provide the best fit, many statistical distributions such as the Weibull (2-parameter, 3-parameter, and bimodal), Gumbel, Normal, Lognormal, Logistic, and G-Gamma ($G = \text{Generalized}$) were initially used to fit the experimental data using the statistical package Reliasoft Weibull++²⁴ and the correlation coefficient and log-likelihood values recorded in each case. The 3-parameter Weibull and G-Gamma distributions were found to consistently provide the best fit of the data and were subsequently chosen for this study. The distribution parameters for both distributions were then estimated using rank regression. For convenience, mathematical formulations of each distribution are summarized below, from Nilakantan et al.²⁵

The probability density function (PDF) of the G-Gamma distribution is given by:

$$f(t) = \frac{\beta}{\Gamma(k)\theta} \left(\frac{t}{\theta}\right)^{k\beta-1} \exp\left(-\left(\frac{t}{\theta}\right)^\beta\right) \quad (3)$$

where $\theta > 0$ is the scale parameter, $\beta > 0$ and $k > 0$ the shape parameters, and $\Gamma(k)$ the gamma function of k . Here t is the variable which represents the tensile strength in units of MPa. However, Weibull++²⁴ uses

a reparameterization with parameters μ , σ , and λ where:

$$\mu = \ln(\theta) + \frac{1}{\beta} \ln\left(\frac{1}{\lambda^2}\right) \quad \sigma = \frac{1}{\beta\sqrt{k}} \quad \lambda = \frac{1}{\sqrt{k}} \quad (4)$$

The PDF can now be represented as:

$$f(t) = \frac{|\lambda|}{\sigma t} \cdot \frac{1}{\Gamma\left(\frac{1}{\lambda^2}\right)} \cdot \exp\left(\frac{\lambda \frac{\ln(t)-\mu}{\sigma} + \ln\left(\frac{1}{\lambda^2}\right) - e^{\lambda \frac{\ln(t)-\mu}{\sigma}}}{\lambda^2}\right) \quad \text{if } \lambda \neq 0 \quad (5a)$$

$$f(t) = \frac{1}{t\sigma\sqrt{2\pi}} \cdot \exp\left(-\frac{1}{2} \left(\frac{\ln(t) - \mu}{\sigma}\right)^2\right) \quad \text{if } \lambda = 0 \quad (5b)$$

The CDF, which is used to obtain the cumulative probability of failure at a particular strength, is given by:

$$F(t) = \Gamma_I\left(\frac{\lambda \left(\frac{\ln(t) - \mu}{\sigma}\right)}{\lambda^2}; \frac{1}{\lambda^2}\right) \quad \text{if } \lambda > 0 \quad (6a)$$

$$F(t) = 1 - \Gamma_I\left(\frac{\lambda \left(\frac{\ln(t) - \mu}{\sigma}\right)}{\lambda^2}; \frac{1}{\lambda^2}\right) \quad \text{if } \lambda < 0 \quad (6b)$$

where $\Gamma_I(k;x)$ is the incomplete gamma function of k and x . The 2-parameter Weibull distribution is actually a special case of the G-Gamma distribution when $\lambda = 1$, $\beta = 1/\sigma$, and $\eta = \ln(\mu)$.²⁴ The CDF is obtained by integrating the PDF of a random variable, in this study the yarn strength, from negative infinity to a particular chosen value. Thus, the CDF represents the total area under the PDF curve up to that particular chosen value, and therefore yields the cumulative probability of finding all yarn strengths less than or equal to the particular chosen value.

The PDF of the 3-parameter Weibull distribution is given by:

$$f(\sigma) = \left(\frac{m}{\sigma_0}\right) \left(\frac{\sigma - x}{\sigma_0}\right)^{m-1} \exp\left(-\left(\frac{\sigma - x}{\sigma_0}\right)^m\right) \quad (7)$$

and the CDF is given by:

$$F(\sigma) = 1 - \exp\left(-\left(\frac{\sigma - x}{\sigma_0}\right)^m\right) \quad (8)$$

where σ_0 is the scale parameter, m the shape parameter, x the threshold parameter, and σ the tensile strength.

In this study, the 3-parameter Weibull distribution was chosen over the 2-parameter and bimodal Weibull distributions as it consistently gave a better fit. The 3-parameter Weibull is usually used when the MR data points do not lie on a straight line when plotted on Weibull probability paper, and display some concavity or convexity. Then x is a number which is subtracted from each of the MR data points in an attempt to make the shifted coordinates fall on a straight line. In such a case, the parameter x has physical significance, and represents the maximum strength below which there is no yarn failure, that is the first instance of failure occurs at a value just greater than x . However, the parameter x may also simply represent another fitting parameter with no physical significance, for example, when x is a negative number. In the case of the 2-parameter Weibull distribution, $x = 0$. The correlation coefficient was used to choose between using either the 3-parameter Weibull or G-Gamma distributions to fit the experimental data.

Results and discussion

Analysis using the yarn strength data

The experimental data and fitted PDF and CDF distributions for the 101.6 and 381.0 mm gage length samples from the three yarn sources are displayed in Figures 6 and 7, respectively. The color symbols in Figures 6(b) and 7(b) represent the MRs assigned to each experimental strength data point, while the color lines represent the fitted CDFs. Due to space limitations, typical plots for only two gage lengths were displayed here. Table 2 lists the type of statistical distribution chosen, the corresponding distribution parameters, as well as the number of tests conducted for all the gage lengths studied. The list of symbols is as follows: spool (*S*), greige fabric warp yarn (*GW*), greige fabric fill yarn (*GF*), scoured fabric warp yarn (*SW*), scoured fabric fill yarn (*SF*), G-Gamma distribution (*GG*), 3-parameter Weibull distribution (*3P*), and correlation coefficient (ρ). The three parameters ($P1-P3$), respectively represent: μ , σ , and λ (for the G-Gamma

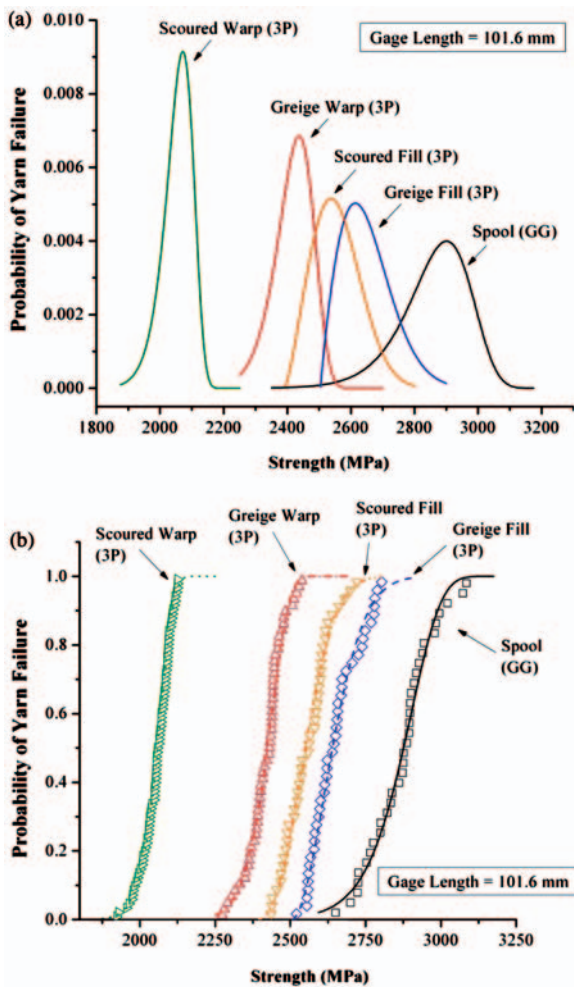


Figure 6. Strength data-based probability distributions for 101.6 mm gage length yarn samples: (a) PDF and (b) CDF.

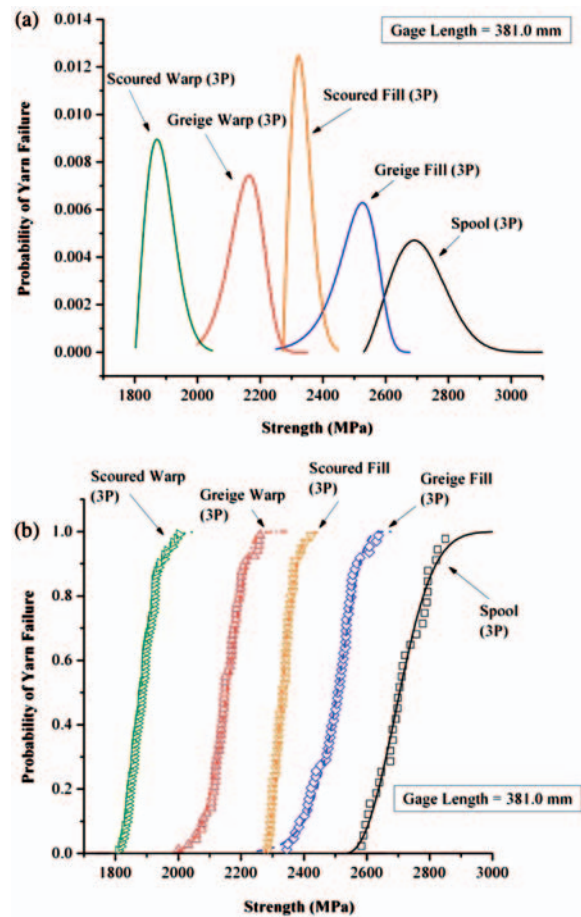


Figure 7. Strength data-based probability distributions for 381.0 mm gage length yarn samples: (a) PDF and (b) CDF.

Table 2. Statistical distribution parameters used to characterize the experimental strength data

Source	GL (mm)	Type	P1	P2	P3	ρ	# tests
S	25.4	GG	8.0232	0.0469	1.0875	0.9997	82
GW	25.4	GG	7.9034	0.0305	1.6562	0.9943	54
GF	25.4	GG	7.9583	0.0388	-0.3248	0.9971	71
SW	25.4	3P	3.0090	194.1927	2161.1911	0.9962	57
SF	25.4	3P	9.1012	796.732	2055.7578	0.9949	49
S	50.8	GG	7.9929	0.0371	0.6890	0.9968	49
GW	50.8	3P	3.8656	365.5862	2192.0415	0.9890	61
GF	50.8	3P	5.5071	615.3447	2209.9266	0.9942	52
SW	50.8	GG	7.7090	0.0332	-0.6434	0.9927	87
SF	50.8	GG	7.8685	0.0369	-0.2487	0.9908	42
S	101.6	GG	7.9739	0.0324	0.8578	0.9976	34
GW	101.6	3P	10.3268	556.9807	1885.7320	0.9910	55
GF	101.6	3P	1.8751	163.9135	2504.7721	0.9832	42
SW	101.6	3P	15.1862	611.7679	1462.4008	0.9970	79
SF	101.6	3P	2.3359	185.9720	2391.1297	0.9889	42
S	254.0	3P	2.1587	194.1650	2588.5251	0.9797	32
S	381.0	3P	2.3666	205.7002	2528.2644	0.9857	30
GW	381.0	3P	6.8500	342.6437	1830.0700	0.9918	61
GF	381.0	3P	56.5784	3308.9500	-781.5434	0.9814	57
SW	381.0	3P	2.0296	96.6988	1801.8559	0.9979	78
SF	381.0	3P	2.0323	69.5570	2272.3400	0.9885	52

S, spool; GW, greige warp; GF, greige fill; SW, scoured warp; SF, scoured fill; ρ , correlation coefficient.

GG, G-Gamma; P1 = μ ; P2 = σ ; P3 = λ .

3P, 3-parameter Weibull; P1 = m ; P2 = σ_0 ; P3 = x .

distribution) and m , σ_0 , and x (for the 3-parameter Weibull distribution).

A number of overall trends can be observed from the results presented in Figure 6. As expected, the control samples taken directly from the spool exhibited the highest yarn strength distributions for a given gage length. Strength distributions generated from warp and fill yarns that were extracted from both fabrics, namely greige and scoured, and tested at the same gage length shifted to lower strength levels. This indicates the presence of weaving strength degradations in the fabric yarns and is more clearly seen when considering the shift in CDF distributions to lower strengths in Figure 6(b).

Closer inspection of the results presented in Figure 6 shows that in both the greige and scoured fabrics, the strengths of the warp yarns were always weaker than the fill yarns. This indicates the warp yarns undergo greater extents of strength degradation than the fill yarns. Recall from Figure 2 that the warp yarns undergo more curvature during weaving that may contribute to additional strength reduction apart from the effects of abrasion.

One also observes from Figures 6 and 7 that the strengths of the warp (and fill) yarns extracted from

the scoured fabric were lower than those of the warp (and fill) yarns from the greige fabric. This indicates that the scouring process further degrades the strengths. Furthermore, scouring degrades the strength of the warp yarns to a greater extent than the fill yarns. One concludes that the scouring of the greige fabric affects the weaving degraded warp yarns to a greater extent than the fill yarns (that have less weaving-induced degradation).

In order to quantify the extent of weaving damages, the strength retention factor (SRF) at a given probability of failure is defined:

$$\text{SRF}_X = \frac{\text{sample strength}}{\text{control sample strength}} \Big|_{\text{at } X\% \text{ cumulative probability of failure}} \quad (9)$$

Table 3 lists the SRFs for the 101.6 mm gage length yarn samples extracted from the greige and scoured fabrics, with all values normalized with respect to their control samples, namely from the spool. The strength retentions have been calculated at 10%, 50%, and 90% cumulative probabilities of failure.

Table 3. SRFs for the 101.6 mm gage length yarn samples

GL = 101.6 mm	Retention at X% cumulative probability of failure		
	10%	50%	90%
Spool	1.00	1.00	1.00
Warp, Greige	0.85	0.84	0.82
Fill, Greige	0.94	0.92	0.92
Warp, Scoured	0.73	0.72	0.70
Fill, Scoured	0.90	0.89	0.88

Table 4. SRFs for the 381.0 mm gage length yarn samples

GL = 381.0 mm	Retention at X% cumulative probability of failure		
	10%	50%	90%
Spool	1.00	1.00	1.00
Warp, Greige	0.80	0.80	0.79
Fill, Greige	0.91	0.93	0.91
Warp, Scoured	0.70	0.70	0.69
Fill, Scoured	0.88	0.86	0.84

At the 50% probability of failure, the greige warp yarn shows a 16% drop in strength while the greige fill shows only an 8% drop. In the case of the scoured warp and fill yarns, the reductions are greater at 28% and 11%, respectively. The difference between the warp and fill yarn strength retentions grows from 8% in the greige fabric to 17% in the scoured fabric. The difference between the strength retentions of the greige and scoured warp yarns is 12% while that of the fill yarns is 3%. This confirms the earlier observations that the scouring process degrades the warp yarns to a greater extent than the fill yarns. Table 4 lists similar information for the 381.0 mm gage length samples. Similar trends are observed for this gage length.

In Tables 3 and 4, the strengths for the 101.6 and 381.0 mm gage length yarns are normalized by the spool strength at that same gage length for each probability of failure to isolate the effect of weaving. Comparing Tables 3 and 4, we do not observe much difference in strength retention at different gage lengths when comparing the same fabric yarn source at the same cumulative probability of failure. For example, the largest difference in strength retentions of 5% is seen when comparing greige warp yarns at a 10% probability of failure for the 101.6 mm (0.85) and 381.0 mm (0.80) gage length cases. The smallest difference in

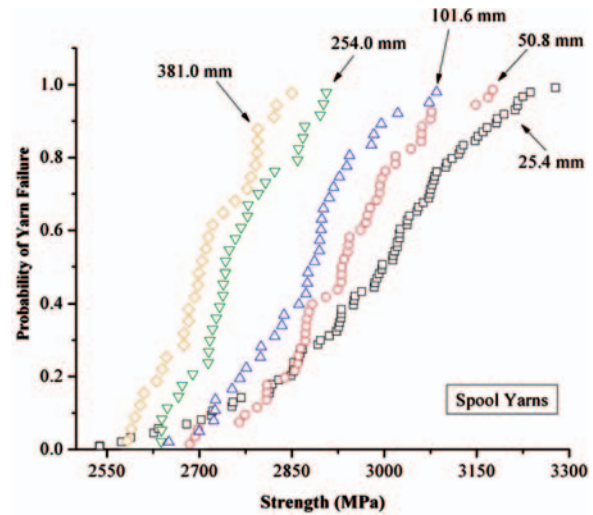


Figure 8. Strength data-based length-scale effects in the spool yarns.

strength retentions is 1% as seen in a few cases. One concludes for this gage length range that the effects of weaving and scouring processes on the strength degradations are independent of gage length. This indicates that length-scale effects and weaving/scouring effects can be considered independent degradation mechanisms as a first approximation.

To study the length-scale effects in greater details, additional gage lengths were tested. Figure 8 displays the experimental strength data of yarns from the spool, in the form of MRs or cumulative probabilities of failure, for each gage length studied (25.4–381.0 mm). The length-scale effects are apparent, with the distributions shifting slightly toward the left or lower strengths and rotating counter clockwise as the gage length increases. Two interesting trends are also apparent. The first trend is that the horizontal gap between the distributions decreases as the gage length increases, indicating the possible presence of a cutoff gage beyond which the strength distributions would collapse onto each other. The second trend is that the distributions become increasingly upright as the gage length increases. This indicates less scatter in the data, as the distributions become more closely clustered around lower mean strengths as the gage length increases. As seen in Figure 8, the strength data of the 25.4 mm gage length show the highest variability, and at lower probabilities of failure (<0.25), the strength data start to overlap that of all the other gage lengths. This behavior is only observed for the 25.4 mm gage length that shows a characteristically different shaped MR data curve. Table 5 lists the SRFs for the spool yarn samples at varying gage lengths, with the data normalized against the 25.4 mm gage length. At the 90% probability of failure the 381.0 mm gage length shows the largest drop of 11% in strength. The drop in retention

decreases with increasing gage lengths, for example there is a 2% drop between the 25.4 and 50.8 mm gage lengths as well as between the 254.0 and 381.0 mm gage lengths at the 50% probability of failure. The reported overlap of the 25 mm gage length data at low probabilities of failure is also apparent in Table 5, where the retentions of the 50.8 and 101.6 mm gage lengths are respectively the same (1.0) and slightly higher (1.02) than the 25.4 mm gage length at the 10% probability of failure, while the 381.0 mm gage length shows only a 5% drop in strength (0.95). Upon comparing the SRFs from Tables 3–5, one concludes that the overall drop in strengths due to length-scale effects alone is lesser than that due to weaving and scouring effects.

Figure 9 displays the combined length-scale and weaving effects for the warp and fill yarns, respectively from the greige and scoured fabrics. Once again, the strengths are seen to decrease with increasing gage lengths; however, the two previous length-scale trends observed in the spool yarns do not appear in these results. Instead of rotating counter clockwise, the strength distributions of these fabric yarns appear to be horizontally translated toward lower strengths. As discussed earlier, this could be a consequence of the weaving process.

The combined effect of length scale with weaving and scouring on the strength retentions can be assessed by using Tables 3 and 4 with Table 5. To illustrate this, we will compare the strength at the 50% probability of failure between the 25.4 mm gage length spool and the 381.0 mm greige warp yarn. For this comparison, by multiplying the retention factor of the 381.0 mm gage length spool yarn with respect to the 25.4 mm gage length spool yarn (0.9) with the retention factor of the 381.0 mm gage length greige warp yarn with respect to the 381.0 mm gage length spool yarn (0.8), we get a net retention of 0.72 which corresponds to a drop in strength of 28%. Similarly, for the combination of length scale, weaving, and scouring effects, we observe a drop of 37% when comparing the 25.4 mm gage

length spool yarn data with the 381.0 mm gage length scoured warp yarn data at the 50% probability of failure. This methodology is possible since the length and weaving degradation mechanisms in our study are either independent or weakly coupled.

It would be useful to be able to predict the strength distribution of a yarn at any gage length by extrapolating from a single gage length to prevent having to run many experiments. To account for the length-scale effects, the factor (L/L_0) is incorporated into Equation (8), where L refers to the current gage length (or length to which the data need to be extrapolated) and L_0 refers to the original gage length (or length at which the experimental testing was conducted).⁴ Thus, Equation (8) becomes:

$$F(\sigma) = 1 - \exp\left(-\left(\frac{L}{L_0}\right)\left(\frac{\sigma - x}{\sigma_0}\right)^m\right) \quad (10)$$

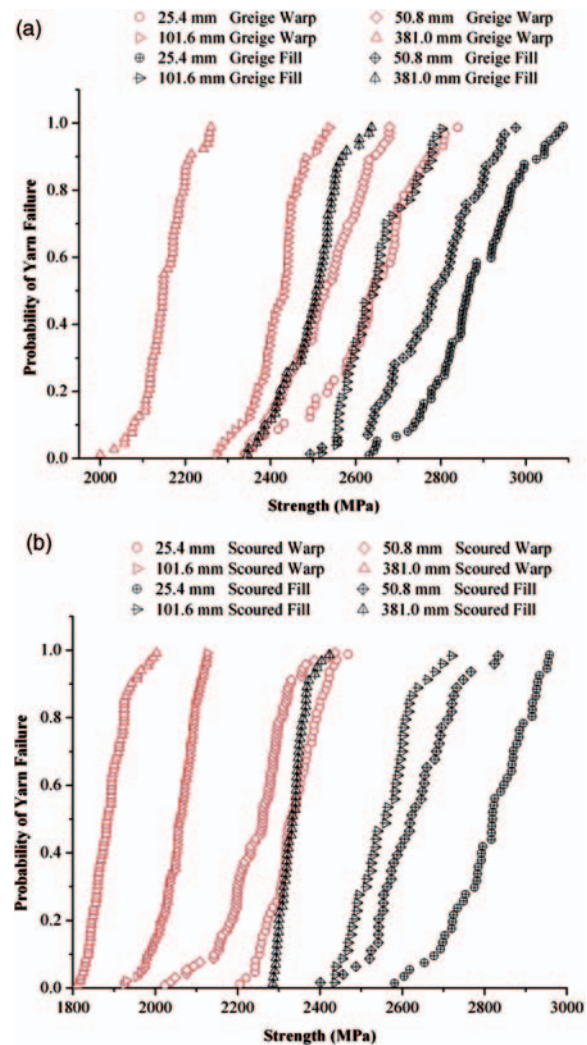


Figure 9. Strength data-based length-scale effects in the yarns from: (a) greige fabric and (b) scoured fabric.

Table 5. SRFs for the spool yarn samples at varying gage lengths

Spool	Retention at X% cumulative probability of failure		
	10%	50%	90%
Gage length (mm)			
25.4	1.00	1.00	1.00
50.8	1.02	0.98	0.97
101.6	1.00	0.96	0.95
254.0	0.97	0.92	0.91
381.0	0.95	0.90	0.89

Since Equation (10) does not consistently work well with all types of fibers, and sometimes overestimates the strength of fibers with length $L < L_0$ and underestimates for $L > L_0$. Wu and Netravali,⁷ reports on the modification made to Equation (10), wherein a factor α is introduced so that the length scaling formulation becomes:

$$F(\sigma) = 1 - \exp\left(-\left(\frac{L}{L_0}\right)^\alpha \left(\frac{\sigma - x}{\sigma_0}\right)^m\right) \quad (11)$$

Here α ranges between 0 and 1. For example, Phoenix et al.¹¹ reports an α value of 0.6 for Kevlar 49 fibers. In attempting to use Equation (10) to fit the data in Figure 8, we find that Equation (10) also tends to either over or under estimate the strengths. However, we also found that using a single value for α in Equation (11) did not consistently work either. Hence, we postulate a new form for α as follows, where:

$$\begin{aligned} \alpha &= \alpha_1 & \text{for } L < L_0 \\ \alpha &= \alpha_2 & \text{for } L > L_0 \\ \alpha &= 1 & \text{for } L = L_0 \end{aligned} \quad (12)$$

Using Equation (12), with $\alpha = 0.764$ for the tests with $L < L_0$ and $\alpha = 1.612$ for $L > L_0$, the experimental strength data (MR data) displayed in Figure 8 are fit using our modified length-scaled 3-parameter Weibull distribution, as shown in Figure 10. The values for α were determined using least squares error estimation. Here the CDF of the 101.6 mm gage length yarn samples from the spool is used to extrapolate the CDFs of the other gage lengths, namely 25.4, 50.8, 254.0, and 381.0 mm, of yarns also extracted from the

spool. As can be seen from Figure 10, overall good fits of the experimental data are achieved. However, only for the 25.4 mm gage length data at low probabilities of failure (< 0.25), the extrapolated CDF tends to overestimate the actual yarn strength.

Although the G-Gamma distribution provided a better fit than the 3-parameter Weibull distribution for the 25.4, 50.8, and 101.6 mm gage length spool-based data as reported in Table 2, the 3-parameter Weibull distribution was instead used for the length-scale formulation presented here. This was done for convenience since the G-Gamma distribution is relatively far more complex, and further an equivalent length-scale formulation has not yet been developed for the G-Gamma distribution.

In order to fit the experimental MR data in Figure 9 where there are large translations in the CDF plots, a more advanced length-scale formulation is required which is presented in section ‘Analysis using the yarn strain energy data’. The length-scale formulation of Equations (11) and (12) essentially rotates the CDF of the gage length chosen as the basis for extrapolation (i.e., L_0) either clockwise or counter clockwise, in an attempt to fit the strength data of the other gage lengths. The direction of rotation depends on whether α and the ratio L/L_0 are greater than or lesser than unity. Thus, the large degrees of translation in the CDF plots seen in Figure 9 cannot be handled by this formulation, or for that matter the reported formulations from the literature.^{3,4,7,11}

Analysis using the yarn strain energy data

So far, the yarn strength distributions have been used as the basis for assessing the tensile performance of yarns and assessing the effects of length-scale and weaving processes. It is assumed that fabric yarns with higher strength distributions would improve the performance of woven fabrics in applications involving impact and penetration resistance. However, there are other important material parameters to consider when assessing the impact performance of fabrics, such as yarn tensile modulus, yarn denier, and filament–filament and yarn–yarn coefficient of friction. For example, frictional interactions between the filaments within a yarn, and between warp and fill yarns have been shown to improve the impact performance through frictional sliding energy dissipations.^{26,27} Figure 11 shows a schematic of an idealized load–extension curve during the quasi-static tensile testing of these yarns. During the ‘loading’ portion of the curve, the load monotonically increases until some peak load. In reality, during the loading portion, a small percentage of filaments may fail. These correspond to weaker filaments and filaments that carry larger loads than the

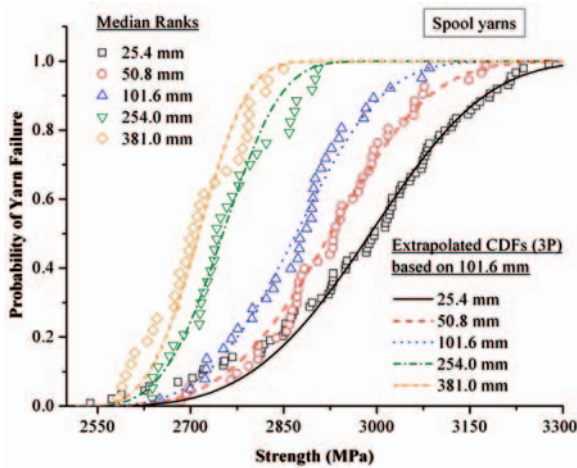


Figure 10. Extrapolated CDFs using the 101.6 mm gage length spool yarn strength data.

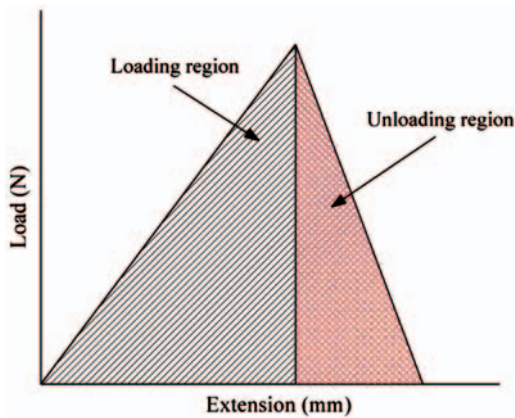


Figure 11. Schematic of an idealized quasi-static yarn load–extension plot.

other filaments. The latter nonuniform loading of filaments is caused by filament misalignment within the yarn. We refer to the region after the peak load as the ‘unloading region,’ see Figure 11. At these quasi-static rates, there is a pronounced unloading region, where the load monotonically drops. In reality, during the unloading region, a majority of filaments begin to progressively fail at different locations along the gage length and the load begins to decrease. Filaments that have failed begin to get pulled apart and in the process slide against other filaments in the yarn. Thus, the unloading region is a consequence of both progressive filament failure as well as filament–filament frictional sliding interactions. The unloading energy, which is obtained from the area underneath the unloading curve, is significant when compared to the loading energy. By considering only the peak tensile strength in the statistical distributions as an indicator of the tensile (or impact) performance, the unloading energy is excluded from consideration, although it could be significant. Therefore in this section, we characterize the total work-to-break for all yarn samples tested earlier, by determining the area underneath the entire load–extension curve. In order to compare results between different gage lengths, the work-to-break has been normalized by the yarn volume; thus, it also corresponds to the SED and has units of mJ/mm^3 or N/mm^2 . By using the work-to-break or SED values instead of only the peak tensile strength, other important energy dissipating mechanisms can be incorporated into the statistical analysis. This is also relevant to the computational modeling of fabrics, where a failure criterion based on tensile strength or SED can be used.

In reality, the load–extension curves do not necessarily monotonically increase or decrease smoothly during the loading and unloading portions, respectively. Further, a sharply defined peak load is not

always obtained. Figure 12 displays seven randomly selected load–extension plots from each yarn source taken during experimental testing. The plots have been corrected for machine compliance. For visual clarity, each plot has been shifted by 0.3 mm to the right. In the spool-based samples, the third curve displays some filament failure accompanied by a small drop in load just before the peak load; however, the other samples show no distinguishable progressive filament failure in the loading region. All the samples have a sharply defined peak load. The unloading region of a few of the samples shows varying degrees of progressive filament failure. In the yarns extracted from the fabric, the greige and scoured warp yarns both display a lack of sharply defined peaks. Progressive failure is clearly seen in the unloading region. In comparison, the greige and scoured fill yarns have better defined peaks. Of the two, the scoured fill yarn samples display very sharp peaks with little to no progressive failure in the unloading region. As can be clearly seen in Figure 12, the area under the unloading region is significant in comparison with the loading region.

Figures 13 and 14 display the experimental SED data, and PDF and CDF distributions, respectively, for the 101.6 and 381.0 mm gage length yarn samples. The color symbols in Figures 13(b) and 14(b) represent the MRs assigned to each experimental SED data point, while the color lines represent the fitted CDFs. A number of interesting trends are apparent, which differ from the trends observed in the corresponding strength data-based plots of Figures 6 and 7. The first interesting trend is that for the same gage length, the yarns from the spool clearly have a much larger scatter than the fabric yarns (wider CDF distribution), unlike the strength-based data, wherein yarns of the same gage length from different sources had similar amounts of scatter. There, the scatter only decreased as a function of increasing gage lengths. The second interesting trend is that the CDF distributions of the yarns extracted from the spool are no longer clear to the right of the greige fabric yarns. In Figure 13(b), the spool yarn CDF overlaps both greige warp and fill yarn CDFs, while in Figure 14(b) the spool yarn CDF is to the left of both greige yarn CDFs. This seems to indicate that there are almost little to no weaving-based degradations in the greige fabric. Clearly, even though the reduced yarn strengths of the greige yarns compared to the spool yarns have resulted in a lower energy in the loading region, this reduction is made up by the energy dissipated during unloading leading to the SED-based spool yarn CDFs either overlapping or lying to the left of the greige yarn CDFs. The third interesting trend is that the difference in extents of damage between the warp and fill yarns is very small with the CDF distributions of the warp and fill yarns from the scoured

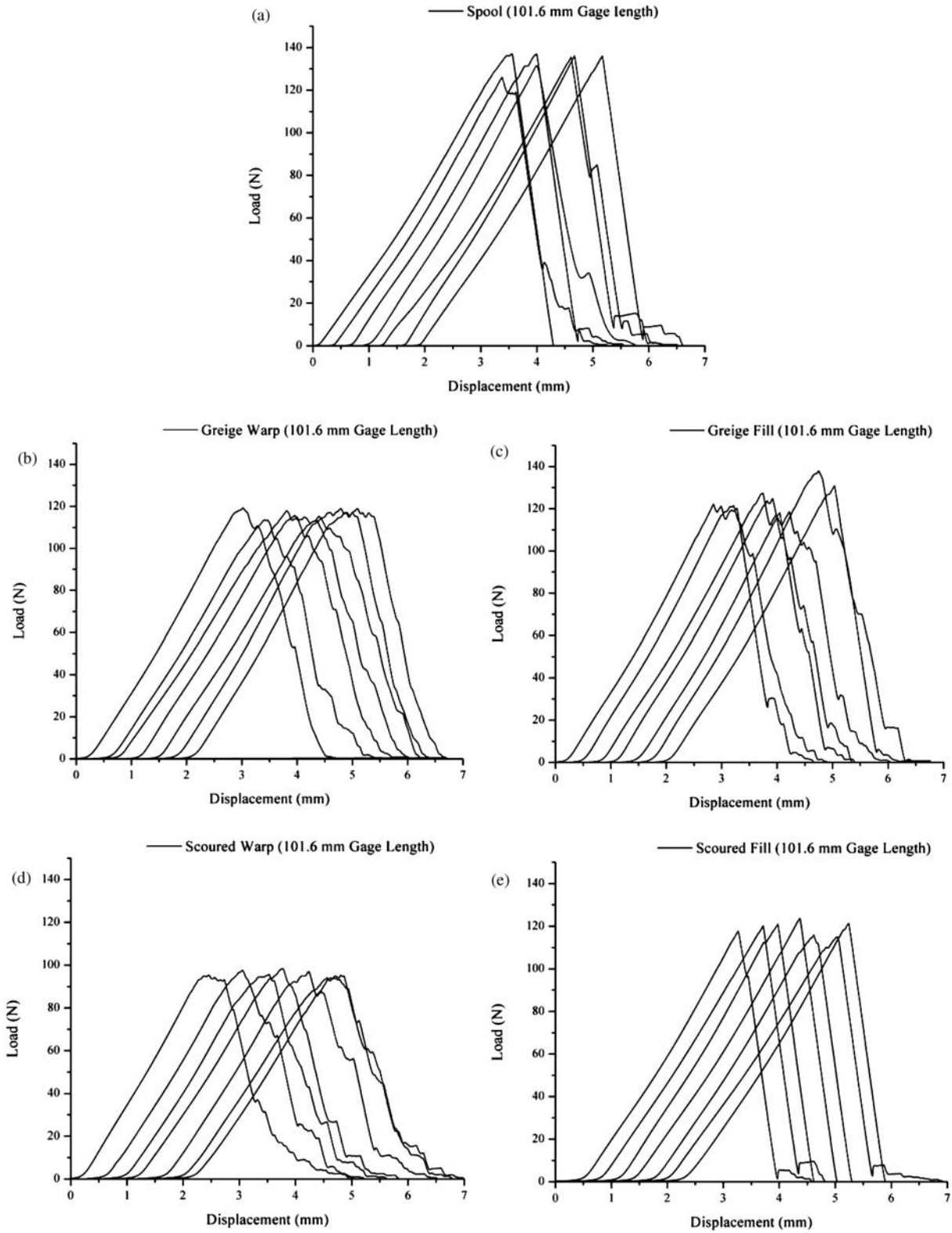


Figure 12. Experimental yarn specimen load–extension plots of: (a) spool, (b) greige warp, (c) greige fill, (d) scoured warp, and (e) scoured fill.

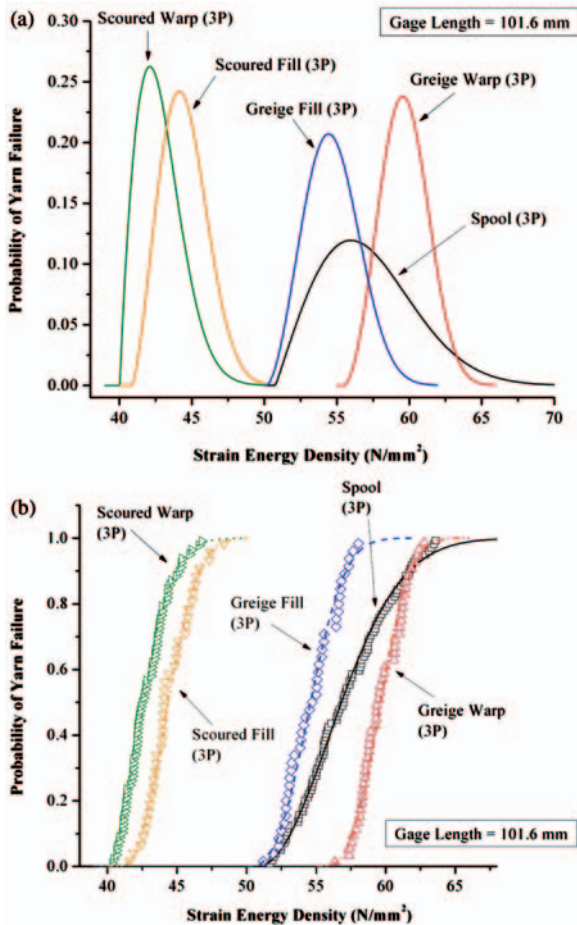


Figure 13. SED data-based probability distributions for 101.6 mm gage length yarn samples: (a) PDF and (b) CDF.

fabric lying close to each other, similar to those from the greige fabric. For example in Figure 13(b), the scoured yarn CDFs are very close to each other while in Figure 14(b) the greige yarn CDFs almost overlap at higher probabilities (>0.5) of yarn failure. When we considered the strength-based data, see Figures 6 and 7, we could clearly observe a greater amount of degradation in the warp yarns compared to the fill yarns. Also, for the same gage length, the gap between the warp yarn CDF and fill yarn CDF was greater in the scoured yarns compared to the greige yarns when considering the strength-based data. However, with the SED-based data, these gaps were sometimes smaller in the scoured yarn CDFs compared to the greige yarn CDFs. Finally, the CDF plots of the greige and scoured yarns are clearly separated from each other with the SED-based data, unlike the strength-based plots, wherein the CDF of the scoured fill yarns used to lie in between the CDF plots of the greige warp and greige fill yarns.

Table 6 lists the type of distribution used, corresponding distribution parameters, and number of tests

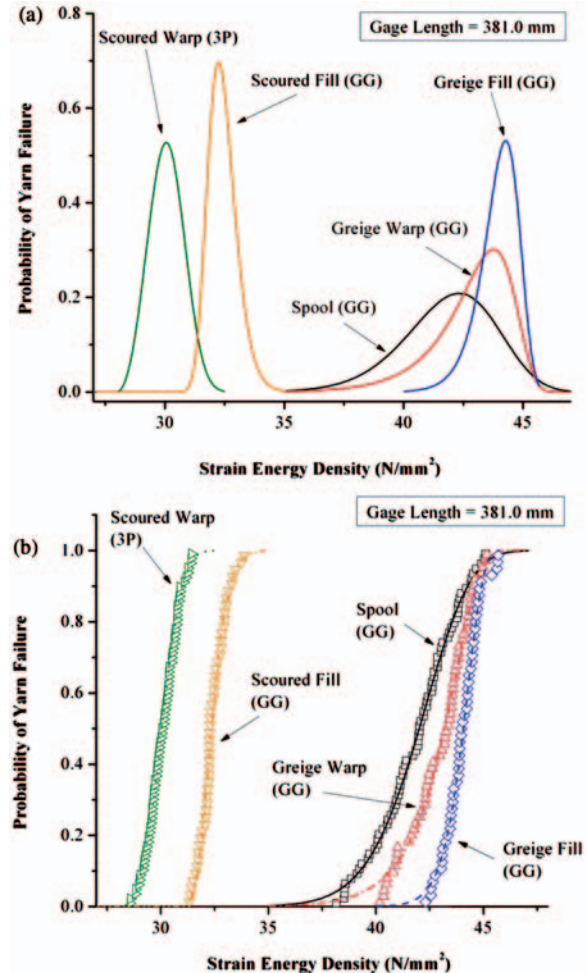


Figure 14. SED data-based probability distributions for 381.0 mm gage length yarn samples: (a) PDF and (b) CDF.

conducted for all cases studied. Tables 7 and 8 list the SED retention factors for the 101.6 and 381.0 mm gage length cases normalized with respect to the spool-based samples for 10%, 50%, and 90% probabilities of failure. Figure 15 displays a side-by-side comparison of the strength and SED-based retention factors for the 101.6 mm gage length case at the 50% probability of failure. For both the cases, the retentions are respectively normalized against their own spool-based strength and SED values. Two surprising observations are noted for the SED-based data as follows. First, as seen in Figure 13(b), the greige warp yarn CDF lies to the right of the greige fill yarn CDF and this is reflected in the retentions reported in Table 7 where the greige warp yarns have higher retentions. Second, the retentions of the greige warp yarns for the 101.6 mm gage length case and the greige warp and fill yarns for the 381.0 mm gage length case show values greater than unity as reported in Tables 7 and 8, implying they are 'superior' to the spool-based yarn samples.

Table 6. Statistical distribution parameters used to characterize the experimental SED data

Source	GL (mm)	Type	P1	P2	P3	ρ	# tests
S	25.4	GG	4.6388	0.0682	-0.2837	0.9946	80
GW	25.4	3P	3.5515	23.3342	90.3441	0.9935	51
GF	25.4	3P	4.2189	36.6028	78.4184	0.9937	69
SW	25.4	3P	2.6267	14.2703	78.5788	0.9954	49
SF	25.4	3P	2.5554	22.8240	71.9196	0.9958	47
S	50.8	GG	4.2816	0.0380	-0.0951	0.9967	41
GW	50.8	GG	4.3749	0.0437	-0.6554	0.9971	61
GF	50.8	3P	2.5188	11.3880	64.1779	0.9936	55
SW	50.8	GG	4.0970	0.0563	-0.4411	0.9935	83
SF	50.8	GG	4.1497	0.0618	0.2303	0.9979	50
S	101.6	3P	2.0361	7.2657	50.7537	0.9946	93
GW	101.6	3P	2.8626	4.7394	55.4684	0.9859	50
GF	101.6	3P	2.6496	5.1104	50.1541	0.9890	43
SW	101.6	3P	1.8553	3.1166	40.0405	0.9970	75
SF	101.6	3P	2.4164	4.0577	40.8752	0.9924	40
S	254.0	3P	5.7993	7.7563	38.7847	0.9923	61
S	381.0	GG	3.7472	0.0438	0.6043	0.9931	72
GW	381.0	GG	3.7796	0.0262	1.3551	0.9902	58
GF	381.0	GG	3.7907	0.0159	0.8832	0.9990	53
SW	381.0	3P	3.1854	2.3473	27.9669	0.9969	75
SF	381.0	GG	3.4738	0.0173	-0.5303	0.9978	50

S, spool; GW, greige warp; GF, greige fill; SW, scoured warp; SF, scoured fill; ρ , correlation coefficient.

GG, G-Gamma; P1 = μ ; P2 = σ ; P3 = λ .

3P, 3-parameter Weibull; P1 = m ; P2 = σ_0 ; P3 = x .

Table 7. SED retention factors for the 101.6 mm gage length yarn samples, considering both loading and unloading regions

GL = 101.6 mm	Retention at X% cumulative probability of failure		
	10%	50%	90%
Spool	1.00	1.00	1.00
Warp, Greige	1.08	1.05	1.00
Fill, Greige	0.98	0.96	0.93
Warp, Scoured	0.77	0.75	0.73
Fill, Scoured	0.80	0.78	0.76

Table 8. SED retention factors for the 381.0 mm gage length yarn samples, considering both loading and unloading regions

GL = 381.0 mm	Retention at X% cumulative probability of failure		
	10%	50%	90%
Spool	1.00	1.00	1.00
Warp, Greige	1.04	1.03	1.01
Fill, Greige	1.09	1.05	1.01
Warp, Scoured	0.74	0.72	0.70
Fill, Scoured	0.81	0.77	0.75

These trends are completely different from the strength-based samples where the spool yarns were consistently stronger than the greige yarns, that is the strength retentions of the greige yarns were less than unity. Clearly, the inclusion of the unloading region into this analysis has caused this difference where progressive filament failure and frictional sliding interactions between the filaments have contributed to this apparent improvement in performance of the greige yarns based on SED. This is also seen in Figure 15 where the

SED-based retentions of the greige yarns are higher than the corresponding strength-based retentions. This also explains the apparent reduction in weaving degradations of the warp yarns compared to the fill yarns, as seen in Figure 15 where the normalized retention factors of the greige warp and fill yarns as well as those of the scoured warp and fill yarns are closer in magnitude to each other when considering SED-based data. Yarn surface treatments, finishes, and additives that may alter the filament frictional interactions are

also responsible for these differences in predictions when using a SED-based approach.

It is assumed that if this SED approach had been applied while only considering the area underneath the loading region, then trends similar to those obtained from the strength-based analysis would be obtained. This assumption is based upon all yarn samples from each source displaying a relatively linear loading path and having similar tensile moduli. For a linear elastic solid, the SED is related to the tensile strength as:

$$SED = \frac{\sigma^2}{2E} \tag{13}$$

where σ is the tensile strength and E the tensile modulus. Therefore, if the modulus remains the same, then the qualitative trends obtained from the strength-based study will hold true for the SED-based study that considers only the loading region. Note that while comparing samples or material sources that display widely varying moduli and high degrees of nonlinearity, we would have also had to apply this SED-based approach to analyze only the loading region. Since this is not the case for the data set in our study, as the tensile modulus remained unchanged, we directly consider the entire area underneath the load–extension curves.

Figure 16 displays the MRs or cumulative probabilities of failure assigned to the experimental SED-data for the yarns from the spool as a function of gage length. Similar to Figure 8, distributions shift to the left with increasing gage lengths and also become more upright. In the strength-based data shown in Figure 8, the CDF distributions seemed to cluster

close to each other at very low probabilities of failure which indicates similar values of the threshold parameters (with regard to the 3-parameter Weibull distribution). The CDF distributions also rotated counter clockwise with increasing gage lengths. However, in Figure 16, the CDF distributions are clearly spaced apart which indicate widely different values of the threshold parameter. As mentioned earlier, in certain cases the threshold parameter can be considered as the maximum strength below which there is no yarn failure, so that yarn failure initiates at strengths just higher than the threshold parameter. Similar to the strength-based data, the CDF distributions in Figure 16 seem to indicate the presence of a cutoff gage length for the spool yarns beyond which all SED-based CDF plots would collapse onto one another.

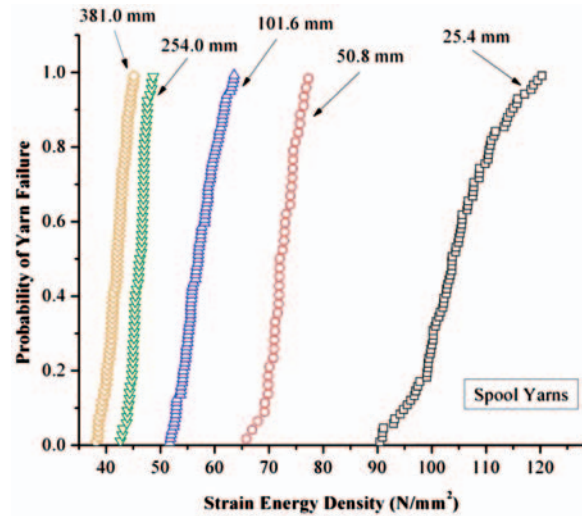


Figure 16. Length-scale effects in the yarns from the spool based on SED data.

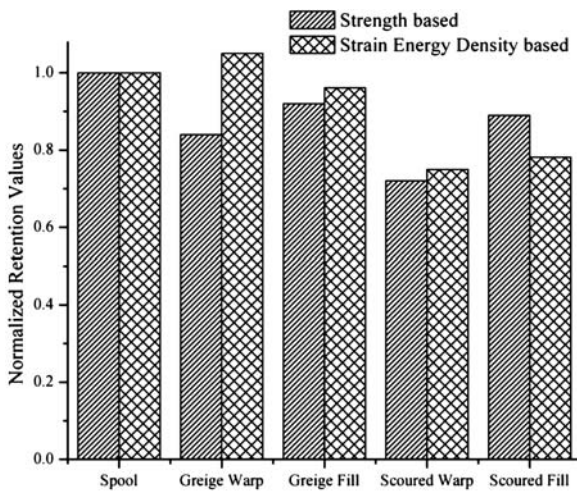


Figure 15. Retention factors for the 101.6 mm gage length yarn samples.

Table 9. SED retention factors for the spool yarn samples at varying gage lengths, considering both loading and unloading regions

Spool	Retention at X% cumulative probability of failure			
	Gage length (mm)	10%	50%	90%
25.4		1.00	1.00	1.00
50.8		0.72	0.70	0.67
101.6		0.56	0.55	0.54
254.0		0.46	0.44	0.42
381.0		0.41	0.40	0.39

Table 9 lists the SED retention factors for the spool yarns at the various gage lengths. The combined effect of both weaving and scouring with length-scale effects on the SED retentions can be assessed by using Tables 7 and 8 with Table 9. For the combination of length-scale and weaving effects, we observe a drop in SED of 59% when comparing the 25.4 mm gage length spool yarn data with the 381.0 mm gage length greige warp yarn data at the 50% probability of failure. Similarly, for the combination of length-scale, weaving, and scouring effects, we observe a drop of 71% when comparing the 25.4 mm gage length spool yarn data with the 381.0 mm gage length scoured warp yarn data at the 50% probability of failure. The drops in SED for these two cases (59% and 71%) are respectively much larger than the drops in strength for the same two cases (28% and 37%). This is because the retention factors due to length-scale effects for the spool yarn samples are much smaller for the SED-based data compared to the strength-based data, as seen by comparing Tables 5 and 9. However, recall from Figure 15 that for the same gage length, the SED-based retentions were higher than the strength-based retentions (except for the scoured fill yarn case), indicating improved tensile performance and lesser weaving degradations.

Upon comparing the SED retention factors from Tables 7–9, one concludes that the overall drop in SED due to length-scale effects is far greater than that due to weaving and scouring effects. This trend is opposite to that observed for the strength-based data and is attributable to the progressive failure of the tows.

Figure 17 displays the SED-based length-scale effects of the greige and scoured fabric yarns. For all gage lengths studied, the CDF plots of the warp and fill yarns are very close to each other for both the greige and scoured fabric cases, sometimes even overlapping one another. An interesting observation noted earlier is that in some cases the warp yarn CDF plots lie to the right of the fill yarn CDF plots, indicating the warp yarns underwent slightly lesser degradations. This did not appear in the strength-based CDF distributions, wherein the warp yarns were consistently and clearly degraded to larger extents compared to the fill yarns. Recall Figure 9 where the strength-based CDF plots of each fabric yarn source considered separately, namely (greige/scoured)–(warp/fill), did not grow closer to each other with increasing gage lengths. Conversely, the SED-based CDF plots for each fabric yarn source presented in Figure 17 grow closer together with increasing gage lengths indicating the presence of a cutoff gage length beyond which all SED-based CDF plots would collapse onto one another.

Comparing Figures 10 and 16, it is evident that both the length-scale formulation from the literature given in Equations (10) and (11) and our new length-scale

formulation given in Equations (11) and (12) cannot be applied to Figure 16. As discussed earlier the term $(L/L_0)^\alpha$ in Equation (11) caused either a clockwise or counter clockwise rotation in the CDF distribution depending on whether the ratio L/L_0 and the parameter α were greater than or lesser than unity. However, in Figure (16) there are large degrees of translation between the SED CDF distributions at different gage lengths indicating threshold distribution parameters (with respect to the 3-parameter Weibull distribution) that significantly vary from each other unlike the strength-based data. Therefore, a new length-scale formulation is required that incorporates this variation in threshold parameter with gage length. Once again, we will consider only the 3-parameter Weibull distribution to develop the new length-scale formulation.

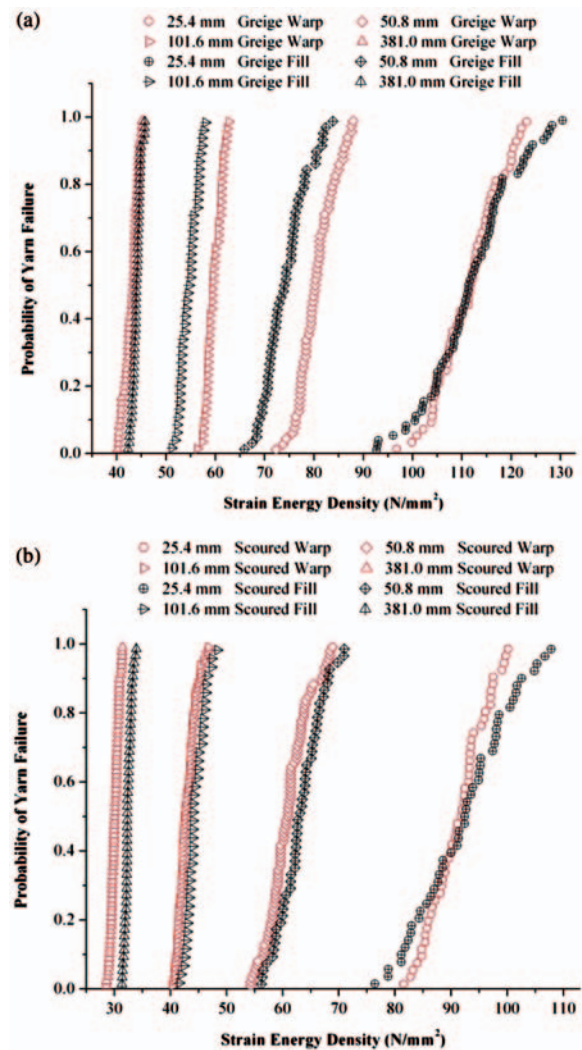


Figure 17. SED data-based length scale effects in the yarns from: (a) greige fabric and (b) scoured fabric.

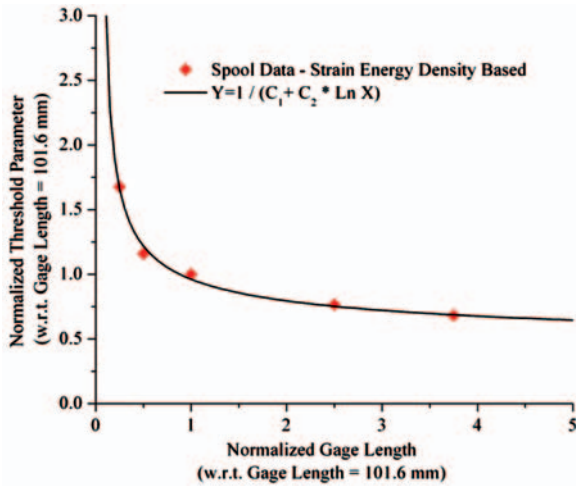


Figure 18. Variation of normalized threshold parameter with normalized gage length for the spool yarn.

Similar to the strength-based length-scaling, we will attempt to use the SED data of the 101.6 mm gage length spool yarn to extrapolate the other spool yarn gage lengths. Figure 18 displays the variation of the normalized threshold parameter (Y) with the normalized gage length (X), where the normalization has been done with respect to the 101.6 mm gage length spool yarn data. The data are fit using the following function:

$$Y = \frac{1}{c_1 + c_2 \ln X} \quad (14)$$

with $c_1 = 1.0404$ and $c_2 = 0.3159$.

Incorporating Equation (14) into Equation (11), we derive our second new length-scale formulation given by:

$$F = 1 - \exp \left[- \left(\frac{L}{L_0} \right)^\alpha \left(\frac{1}{\sigma_0} \right)^m \left(\sigma - x \left(\frac{1}{c_1 + c_2 \ln \left(\frac{L}{L_0} \right)^\beta} \right) \right)^m \right] \quad (15)$$

Similar to the α parameter, another parameter β is used with the L/L_0 term that scales the threshold parameter. The form of β is similarly given by:

$$\begin{aligned} \beta &= \beta_1 & \text{for } L < L_0 \\ \beta &= \beta_2 & \text{for } L > L_0 \\ \beta &= 1 & \text{for } L = L_0 \end{aligned} \quad (16)$$

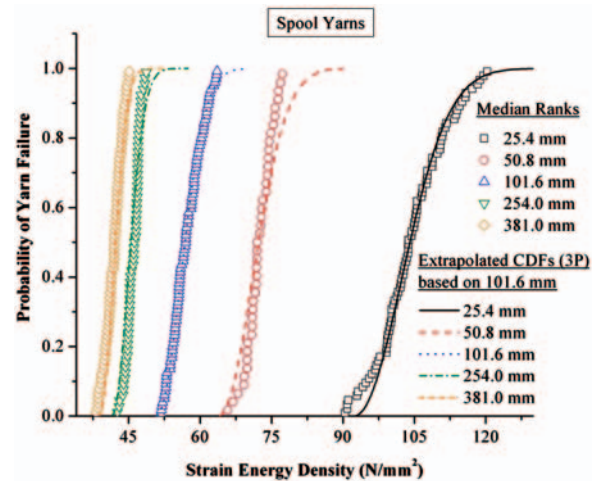


Figure 19. Extrapolated CDFs using the 101.6 mm gage length spool yarn SED data.

Using Equation (15) with Equations (12) and (16), with $\alpha = 0.974$ and $\beta = 1.120$ for the gage lengths with $L < L_0$, and $\alpha = 0.920$ and $\beta = 0.636$ for $L > L_0$, the experimental SED data (MR data) displayed in Figure 16 are fit using our second modified length-scaled 3-parameter Weibull distribution, as shown in Figure 19. The values for α and β were determined using least squares error estimation. Here the CDFs of the 101.6 mm gage length yarn samples from the spool are used to extrapolate the SED-based CDF plots of the other gage lengths, namely 25.4, 50.8, 254.0, and 381.0 mm, of yarns also extracted from the spool. As can be seen from Figure 19, good fits of the MR data are achieved. However, the extrapolated CDF for the 50.8 mm gage length case shows some deviation from the MR data at high probabilities of failure (>0.85). Different curve fitting functions can be used in our modified length-scale formulation by simply replacing Equation (14) with the desired fitting function. Equation (15) is a flexible function that provides for both rotation and translation of the CDF distributions in either direction. Therefore, it can be further applied to fit the MR data shown in Figures 9 and 17, thereby providing a robust means of accounting for length-scale effects for both strength and SED-based data.

For completeness, Table A1 in the Appendix lists the mean, standard deviation (SD), and coefficient of variation (CV) of the raw experimental data for both the strength- and SED-based data sets. Since the data were best fit using distributions such as the G-Gamma and 3-parameter Weibull distributions which are not symmetric about the mean (such as the

Normal distribution), the reported means do not necessarily correspond to 50% probabilities of yarn failure.

Conclusions

The experimental tensile strength distributions of 600 den Kevlar KM2 yarns under quasi-static loading conditions were obtained at varying gage lengths for yarns obtained from a spool, and extracted from the warp and fill directions of greige and scoured Kevlar S706 fabrics. 3-Parameter Weibull and G-Gamma distributions were used to statistically characterize the strength data as they consistently provided the best fit. Weaving strength degradations were present to a greater extent in the warp yarns compared to the fill yarns, and the scouring process further degraded the strengths compared to the greige fabric. The strength distributions shifted to lower strengths as the gage length increased. A new length-scale formulation based on the 3-parameter Weibull distribution was proposed to account for the length-scale effects and provided good data fits by comparing data extrapolated from a single gage length to the original experimental data corresponding to different gage lengths. In addition to characterizing the strength data, the work-to-break normalized by the yarn volume or SED data was also characterized. This accounted for both the progressive filament failure as well as filament frictional sliding effects. The energy associated with the 'unloading' region of the load-extension plot was significant compared to the energy of the 'loading' region. The SED distributions also shifted to lower values with increasing gage lengths. The CDF distributions of the SED for the warp yarns were located very close to the fill yarns indicating the relative extents of weaving degradations in the warp yarns compared to the fill yarns was far less when considering SED-based data. In some cases, the greige warp yarn CDF was even located to the right of the greige fill yarn CDF. The greige warp and fill yarns showed an improved tensile performance over the spool yarns when considering the SED-based CDF plots. These differences in trends compared to those observed in the strength-based analysis are attributed to incorporating the progressive filament failure and filament frictional sliding interactions into the analysis. The advantage of using the SED-based approach is that different mechanisms of energy dissipation, for example that could be vital to predicting the impact performance of these yarns, can be incorporated into the statistical analysis, thereby providing a more comprehensive treatment. It is expected that other effects such as material nonlinearity and strain rate sensitivity can also be easily included into the analysis while making comparisons between

samples obtained from different sources and of different gage lengths. Also highlighted by this approach was that yarn surface treatments, finishes, and additives could play a vital role in improving the tensile performance. Even though the peak strength may be diminished by weaving processes, the loss in tensile performance could be attenuated by filament frictional interactions. For example, the surface filaments in a yarn may become damaged by abrasion mechanisms during weaving, while other filaments may become affected by curvature induced compression kink band formations and thereby fail earlier; however, by virtue of the subsequent filament frictional sliding interactions, they will still contribute to the overall energy dissipations. This also leads to the exciting possibilities of creating hybridized yarns comprised of filaments of different materials and surface treatments that retain high tensile strengths and exploit these additional energy absorbing mechanisms.

A second new length-scale formulation was proposed to account for the length-scale effects observed in the SED-based data. This was accomplished by scaling the threshold parameter based on the normalized gage length and introducing a second new parameter ' β '. This allowed the extrapolated CDF distributions to both rotate and translate in either direction providing additional flexibility to the formulation. The second new length-scale formulation was also based on the 3-parameter Weibull distribution and provided a good fit of the experimental data at varying gage lengths. The two length-scale formulations proposed in this study allow the prediction of strength and SED-based distributions at any gage length by extrapolating from a single gage length, provided the extrapolated gage lengths are around the single gage length used. The strength-based MR data of the spool yarns and SED-based MR data of the spool and fabric yarns seemed to indicate the presence of a cutoff gage length beyond which all CDF plots would collapse onto one another. This was concluded as a consequence of the gap between the CDF plots becoming narrower with an increase in gage length.

One goal of understanding the extent of material variability in the yarns of a fabric is to correlate the effect of statistical yarn material properties on the probabilistic performance of flexible fabrics, which could then help determine if the fabric impact performance is more governed by the strength or SED distributions of the constituent yarns. Such insight would also be applicable to computational fabric impact simulations that commonly use failure criteria based on strength and SED. All experiments in this study were performed at quasi-static rates. It would also be very interesting to recreate this study at medium ($\sim 100 \text{ s}^{-1}$) and high strain rates ($\sim 1300 \text{ s}^{-1}$) seen during actual fabric

impact to quantify the change, if any, in the magnitudes and trends reported in this study.

Acknowledgments

This study was financially supported by the Army Research Laboratory (ARL), Aberdeen Proving Grounds, MD, USA through the Composite Materials Research (CMR) program at the Center for Composite Materials (CCM), University of Delaware. The authors are particularly grateful to Dr Eric D. Wetzel (ARL) for providing the Kevlar material used for experimental testing and for many helpful technical discussions. The authors gratefully acknowledge Dr Joseph M. Deitzel (CCM) for his technical input to this study and Mr Cameron Showell (CCM) for his assistance with the experimental testing conducted.

References

1. Steenbakkens LW and Wagner HDE. Elasticity and mechanical breakdown of Kevlar 149 aramid fibres by a probabilistic approach. *J Mater Sci Lett* 1988; 7(11): 1209–1212.
2. Wang Y and Xia Y. Experimental and theoretical study on the strain rate and temperature dependence of mechanical behavior of Kevlar fiber. *Composites Part A* 1999; 30: 1251–1257.
3. Schwartz P, Netravali A and Sembach S. Effects of strain rate and gauge length on the failure of ultra-high strength polyethylene fibers. *Text Res J* 1986; 56(8): 502–508.
4. Goda K and Fukunaga H. The evaluation of the strength distribution of silicon carbide and alumina fibres by a multi-modal Weibull distribution. *J Mater Sci* 1986; 21(12): 4475–4480.
5. Farsi Dooraki B, Nemes JA and Bolduc M. Study of parameters affecting the strength of yarns. *J Phys IV France* 2006; 134: 1183–1188.
6. Amaniampong G and Burgoyne CJ. Statistical variability in the strength and failure strain of aramid and polyester yarns. *J Mater Sci* 1994; 29(19): 5141–5152.
7. Wu HF and Netravali AN. Weibull analysis of strength-length relationships in single Nicalon SiC fibres. *J Mater Sci* 1992; 27(12): 3318–3324.
8. Loidl D, Paris O, Rennhofer H, Müller M and Peterlik H. Skin-core structure and bimodal Weibull distribution of the strength of carbon fibers. *Carbon* 2007; 45(14): 2801–2805.
9. Leal AA, Deitzel JM and Gillespie Jr JW. Assessment of compressive properties of high performance organic fibers. *Compos Sci Technol* 2007; 67: 2786–2794.
10. Watson A and Smith R. An examination of statistical theories for fibrous materials in the light of experimental data. *J Mater Sci* 1985; 20(9): 3260–3270.
11. Phoenix SL, Schwartz P and Robinson HHI. Statistics for the strength and lifetime in creep-rupture of model carbon/epoxy composites. *Compos Sci Technol* 1988; 32: 81–120.
12. Haque A, Mahmood S, Walker L and Jeelani S. Moisture and temperature induced degradation in tensile properties of Kevlar-graphite/epoxy hybrid composites. *J Reinf Plast Compos* 1991; 10(2): 132–145.
13. Auerbach I. Kinetics for the tensile strength degradation of nylon and kevlar yarns. *J Appl Polym Sci* 1989; 37(8): 2213–2227.
14. O'Neil JM. Factors contributing to the degradation of PBO fibers under elevated temperature and humidity conditions. Master of Science Thesis, Department of Mechanical Engineering, Texas A&M University, USA, August 2006.
15. Said MA, Dingwall B, Gupta A, Seyam AM, Mock G and Theyson T. Investigation of ultra violet (UV) resistance for high strength fibers. *Adv Space Res* 2006; 37(11): 2052–2058.
16. Gu H. Ultraviolet treatment on high performance filaments. *Mater Des* 2005; 26(1): 47–51.
17. Dobb MG, Robson RM and Roberts AH. The ultraviolet sensitivity of Kevlar 149 and Technora fibres. *J Mater Sci* 1993; 28(3): 785–788.
18. Lee L, Rudov-Clark S, Mouritz AP, Bannister MK and Herszberg I. Effect of weaving damage on the tensile properties of three-dimensional woven composites. *Compos Struct* 2002; 57: 405–413.
19. Abu-Obaid A, Andersen SM, Gillespie Jr JW, et al. Effects of weaving on S-2 glass tensile strength distributions. In: *9th International Conference on Textile Composites*, Newark, DE, USA, 13–15 October, 2008.
20. Abu-Obaid A, Andersen SM, Gillespie Jr JW, et al. Effects of 3D weaving on tensile strength retention of Z-tows. In: *Second World Conference on 3D Fabrics and their Applications*, Greenville, South Carolina, USA, 6–7 April, 2009.
21. Dobb MG, Johnson DJ and Saville BP. Compressional behavior of Kevlar fibers. *Polymer* 1981; 22: 960–965.
22. Hill R and Okoroafor EU. Weibull statistics of fibre bundle failure using mechanical and acoustic emission testing: the influence of interfibre friction. *Composites* 1995; 26(10): 699–705.
23. Wang Y and Xia Y. The effects of strain rate on the mechanical behavior of Kevlar fiber bundles: an experimental and theoretical study. *Composites Part A* 1998; 29A: 1411–1415.
24. Weibull++ Version 7, Reliasoft Corporation, <http://weibull.reliasoft.com>.
25. Nilakantan G, Showell C, Abu-Obaid A, et al. An experimental and numerical study of the impact response (V_{50}) of flexible plain weave fabrics: accounting for statistical distributions of yarn strength. In: *1st Joint American-Canadian International Conference on Composites and the 24th Annual ASC Technical Conference*, University of Delaware, Newark, DE, USA, 15–17 September, 2009.
26. Briscoe BJ and Motamedi F. Role of interfacial friction and lubrication in yarn and fabric mechanics. *Text Res J* 1990; 60(12): 697–708.
27. Duan Y, Keefe M, Bogetti TA, Cheeseman BA and Powers B. A numerical investigation of the influence of friction on the energy absorption by a high-strength fabric subjected to ballistic impact. *Int J Impact Eng* 2006; 32: 1299–1312.

Appendix

The mean (μ), standard deviation (σ), and coefficient of variation (CV) for the strength (subscript 1) and strain energy density (subscript 2) based experimental data sets are listed in Table A1.

Table A1. Some statistical properties of the raw experimental data sets

Source	GL (mm)	# tests	Mean strength, μ_1 (MPa)	SD, σ_1 (MPa)	$CV_1 = \sigma_1/\mu_1$ (%)	# tests	Mean SED, μ_2 (N/mm ²)	SD, σ_2 (N/mm ²)	$CV_2 = \sigma_2/\mu_2$ (%)
S	25.4	82	2981.93	155.56	5.22	80	104.54	7.19	6.88
GW	25.4	54	2628.55	121.15	4.61	51	111.33	6.38	5.73
GF	25.4	71	2873.74	109.90	3.82	69	111.69	8.77	7.85
SW	25.4	57	2334.32	60.92	2.61	49	91.21	4.93	5.41
SF	25.4	49	2811.19	96.23	3.42	47	92.10	8.07	8.76
S	50.8	49	2928.57	115.99	3.96	41	72.43	2.69	3.72
GW	50.8	61	2522.63	94.05	3.73	61	80.58	3.66	4.54
GF	50.8	52	2778.14	114.54	4.12	55	74.26	4.26	5.74
SW	50.8	87	2244.15	81.70	3.64	83	60.98	3.59	5.89
SF	50.8	42	2625.47	94.17	3.59	50	63.12	3.75	5.94
S	101.6	34	2868.82	104.51	3.64	93	57.16	3.16	5.53
GW	101.6	55	2416.67	60.26	2.49	50	59.68	1.56	2.61
GF	101.6	42	2648.99	78.09	2.95	43	54.68	1.80	3.29
SW	101.6	79	2053.63	46.55	2.27	75	42.81	1.55	3.61
SF	101.6	42	2555.21	72.36	2.83	40	44.46	1.59	3.57
S	254.0	32	2759.15	80.52	2.92	61	45.97	1.40	3.05
S	381.0	30	2709.35	76.87	2.84	72	41.89	1.81	4.32
GW	381.0	61	2150.37	53.77	2.50	58	42.96	1.39	3.23
GF	381.0	57	2495.35	69.59	2.79	53	44.01	0.80	1.81
SW	381.0	78	1887.22	43.49	2.30	75	30.06	0.71	2.35
SF	381.0	52	2333.85	31.78	1.36	50	32.41	0.60	1.84